



This is a repository copy of *Structural and functional characterization of IdiA/FutA (Tery_3377), an iron-binding protein from the ocean diazotroph Trichodesmium erythraeum.*

White Rose Research Online URL for this paper:
<http://eprints.whiterose.ac.uk/142090/>

Version: Published Version

Article:

Polyviou, D., Machelett, M.M., Hitchcock, A. et al. (5 more authors) (2018) Structural and functional characterization of IdiA/FutA (Tery_3377), an iron-binding protein from the ocean diazotroph *Trichodesmium erythraeum*. *Journal of Biological Chemistry*, 293 (47). pp. 18099-18109. ISSN 0021-9258

<https://doi.org/10.1074/jbc.RA118.001929>

Reuse

This article is distributed under the terms of the Creative Commons Attribution (CC BY) licence. This licence allows you to distribute, remix, tweak, and build upon the work, even commercially, as long as you credit the authors for the original work. More information and the full terms of the licence here:
<https://creativecommons.org/licenses/>

Takedown

If you consider content in White Rose Research Online to be in breach of UK law, please notify us by emailing eprints@whiterose.ac.uk including the URL of the record and the reason for the withdrawal request.



eprints@whiterose.ac.uk
<https://eprints.whiterose.ac.uk/>



Structural and functional characterization of IdiA/FutA (Tery_3377), an iron-binding protein from the ocean diazotroph *Trichodesmium erythraeum*

Received for publication, April 10, 2018, and in revised form, August 31, 2018. Published, Papers in Press, September 14, 2018, DOI 10.1074/jbc.RA118.001929

Despo Polyviou^{†1}, Moritz M. Machelett^{‡§1}, Andrew Hitchcock^{‡1,2}, Alison J. Baylay[‡], Fraser MacMillan[¶], C. Mark Moore[‡], Thomas S. Bibby[‡], and Ivo Tews^{§3}

From the [†]Ocean and Earth Sciences, National Oceanography Centre Southampton, University of Southampton, Southampton SO14 3ZH, United Kingdom, the [§]Department of Biological Sciences, Faculty of Natural and Environmental Sciences, Institute for Life Sciences, University of Southampton, Southampton SO17 1BJ, United Kingdom, and the [¶]School of Chemistry, University of East Anglia, Norwich NR4 7TJ, United Kingdom

Edited by Norma M. Allewell

Atmospheric nitrogen fixation by photosynthetic cyanobacteria (diazotrophs) strongly influences oceanic primary production and in turn affects global biogeochemical cycles. Species of the genus *Trichodesmium* are major contributors to marine diazotrophy, accounting for a significant proportion of the fixed nitrogen in tropical and subtropical oceans. However, *Trichodesmium* spp. are metabolically constrained by the availability of iron, an essential element for both the photosynthetic apparatus and the nitrogenase enzyme. Survival strategies in low-iron environments are typically poorly characterized at the molecular level, because these bacteria are recalcitrant to genetic manipulation. Here, we studied a homolog of the iron deficiency-induced A (IdiA)/ferric uptake transporter A (FutA) protein, Tery_3377, which has been used as an *in situ* iron-stress biomarker. IdiA/FutA has an ambiguous function in cyanobacteria, with its homologs hypothesized to be involved in distinct processes depending on their cellular localization. Using signal sequence fusions to GFP and heterologous expression in the model cyanobacterium *Synechocystis* sp. PCC 6803, we show that Tery_3377 is targeted to the periplasm by the twin-arginine translocase and can complement the deletion of the native *Synechocystis* ferric-iron ABC transporter periplasmic binding protein (FutA2). EPR spectroscopy revealed that purified recombinant Tery_3377 has specificity for iron in the Fe³⁺ state, and an X-ray crystallography-determined structure uncovered a functional iron substrate-binding

domain, with Fe³⁺ pentacoordinated by protein and buffer ligands. Our results support assignment of Tery_3377 as a functional FutA subunit of an Fe³⁺ ABC transporter but do not rule out dual IdiA function.

Photosynthetic organisms have a higher requirement for iron than heterotrophs because of the dependence of multiple components of the photosynthetic electron transport chain on this essential element (1, 2). This requirement is amplified in nitrogen-fixing cyanobacteria (diazotrophs) because iron is also required by the nitrogenase enzyme (3–5). Therefore, marine diazotrophic cyanobacteria species such as the globally significant *Trichodesmium* have developed diverse strategies that permit survival at the fluctuating or chronically depleted iron concentrations typically encountered in the surface waters of the tropical and subtropical oceans (5–9). *Trichodesmium* accounts for approximately half of the total marine nitrogen fixation (10), supplying both biologically available nitrogen and fixed carbon to oligotrophic ecosystems (11). Physiological experiments suggest *Trichodesmium* can acquire iron from diverse sources (7, 12), and analysis of its genome reveals homologs to iron-uptake systems, such as FeoAB for ferrous (Fe²⁺) iron uptake and the periplasmic ferric hydroxamate-binding protein FhuD (5). Although “omic” studies and similarity to homologous systems in other bacteria can be used to infer function, the inability to genetically engineer *Trichodesmium* means no iron-uptake mechanisms have been directly characterized *in vivo*, limiting our understanding of how this important species has adapted to acquire iron from its environment.

Ubiquitous in cyanobacterial genomes and present in *Trichodesmium* are homologs of a protein variably referred to in the literature as IdiA (iron deficiency-induced) or FutA (ferric uptake transporter). IdiA/FutA-like proteins are synthesized under iron limitation in marine and freshwater cyanobacteria (13, 14) and as such are commonly exploited as *in situ* markers of iron stress (15–17). Despite this, functional assignment of these proteins is presently ambiguous. Homologs can have an intracellular localization (18) and are proposed to be associated with the cytoplasmic side of the thylakoid mem-

This work was supported by a studentship from Natural Environment Research Council (NERC) (to D. P.), funds from the Graduate School of the National Oceanography Centre Southampton (to D. P.) and A. G. Leventis Foundation (to D. P.), and a studentship from the National Oceanography Centre and Biological Sciences, University of Southampton (to M. M. M.). The authors declare that they have no conflicts of interest with the contents of this article.

✂ Author's Choice—Final version open access under the terms of the Creative Commons CC-BY license.

This article contains Tables S1–S3, Figs. S1–S3, and references.

The atomic coordinates and structure factors (codes 6G7N, 6G7P, and 6G7Q) have been deposited in the Protein Data Bank (<http://www.pdb.org/>).

¹ These authors contributed equally to this work.

² Present address: Dept. of Molecular Biology and Biotechnology, University of Sheffield, Firth Ct., Western Bank, Sheffield S10 2TN, United Kingdom.

³ To whom correspondence should be addressed. Tel.: 44-23-8059-4415; E-mail: Ivo.Tews@soton.ac.uk.

Structure and function of *Trichodesmium* Tery_3377

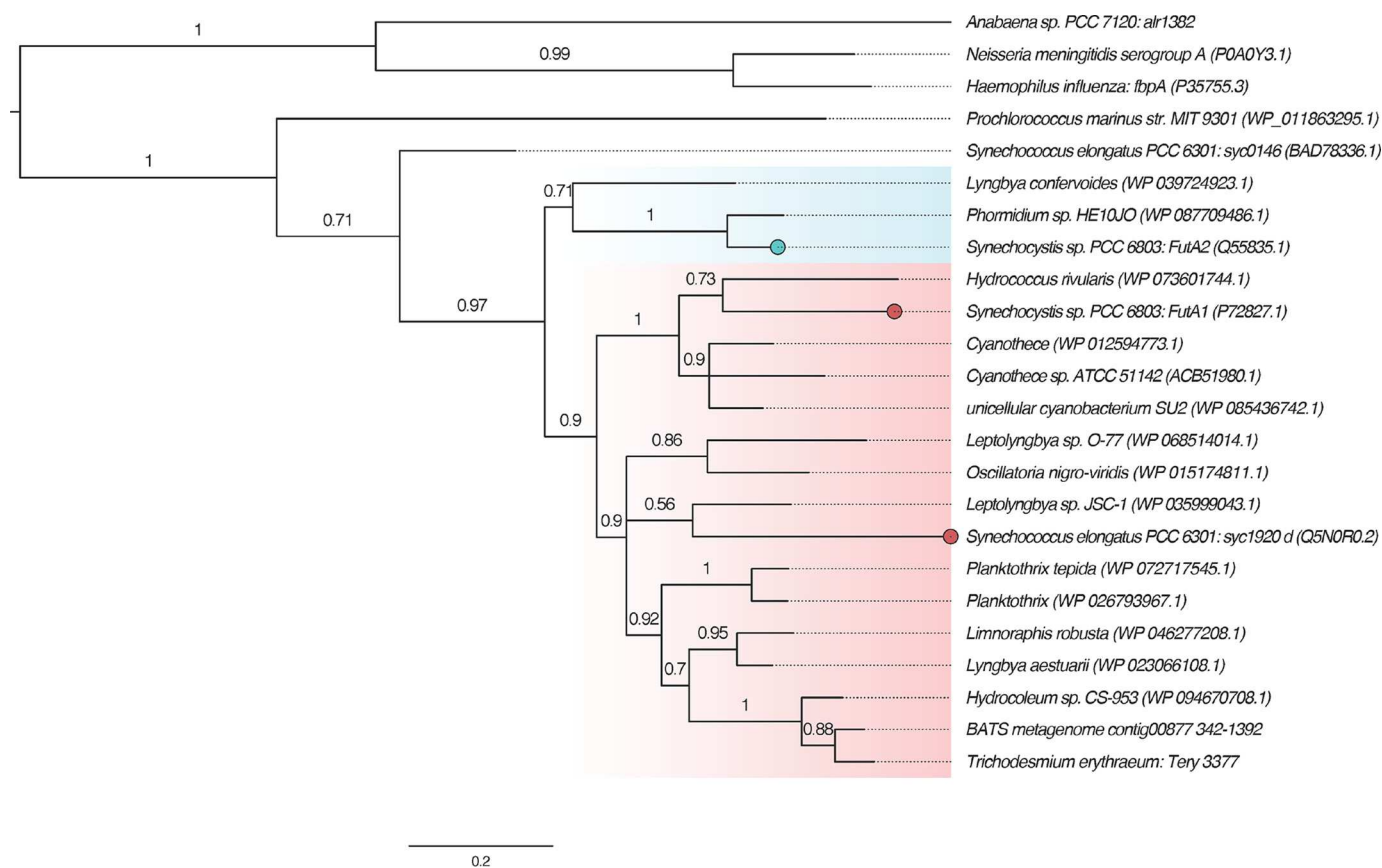


Figure 1. Maximum likelihood phylogenetic analysis of Tery_3377 homologs, based on amino acid sequence. Homologs of Tery_3377 and *Synechocystis* FutA1 and FutA2 were identified using BlastP (40) and aligned along with sequences from the cyanobacteria *S. elongatus* PCC 6301, *P. marinus* MIT 9301, and *Anabaena* PCC 7120, and the pathogenic bacteria *H. influenzae* and *N. meningitidis*. The graphical representation was produced using FigTree v1.4.3, and branch probabilities reported are calculated using an approximate likelihood ratio test (47). The *Synechocystis* FutA1 (red) and FutA2 (blue) proteins are separated into two groups, and Tery_3377 clusters within the FutA1-like group. Filled circles represent branches of the tree for which there is experimental evidence of intracellular (red) or iron transport (blue) function. Database accessions for each protein (SwissProt where possible, otherwise RefSeq) are given in parentheses. The scale bar represents the number of substitutions per site.

brane to protect the acceptor side of photosystem II (PSII)⁴ against oxidative damage during iron stress (18, 19). However, the same protein is also homologous to ferric binding proteins of ATP-binding cassette (ABC) transporters, found in some pathogenic bacteria and several cyanobacteria (20–22).

In the model freshwater cyanobacterium *Synechocystis* sp. PCC 6803 (hereafter *Synechocystis*), there are two characterized paralogs of IdiA/FutA, referred to as FutA1 (Slr1295) and FutA2 (Slr0513). FutA1 has a predominantly intracellular localization, associating with the thylakoid membrane, although it has also been found in the cytoplasmic membrane. In contrast, the FutA2 protein is a periplasmic substrate-binding protein associated with partner FutB and FutC subunits to form an active Fe³⁺ uptake ABC transporter (22–26).

Trichodesmium erythraeum IMS101 encodes only one IdiA/FutA homolog in its genome, Tery_3377 (17). Increased expression/production under iron stress has been reported at both the transcriptional (3, 17), and protein levels (5, 13). Tery_3377 is therefore thought to play an important role in iron homeostasis.

In this study we investigated the role of Tery_3377 to understand whether it is performing a periplasmic function (FutA2-like) or an intracellular function (FutA1-like). We produced Tery_3377 in *futA1* and *futA2* mutants in the genetically tractable model cyanobacterium *Synechocystis* sp. PCC 6803 testing for complementation of mutant phenotypes. We also used signal peptide fusions to GFP to give insight into the cellular localization of Tery_3377. Further, we overproduce and purify recombinant Tery_3377 and confirm ferric iron (Fe³⁺) coordination by electron paramagnetic resonance (EPR) spectroscopy and structure determination, classifying Tery_3377 as a class IV iron substrate-binding domain (27). This functional and structural investigation of Tery_3377 helps to characterize its role in the iron-stress physiology of a globally significant microbe and suggests a potential need to reassess the roles of FutA/IdiA family proteins more generally.

Results

Insights from sequence analysis

The protein sequence of the Tery_3377 protein is 58 and 57% identical to *Synechocystis* FutA1 and FutA2, respectively (Table S1). In *Synechocystis*, FutA1 and FutA2 are 52% identical to one another (21) yet appear to have distinct cellular function. Functional assignment based on primary sequence comparisons is

⁴ The abbreviations used are: PSII, photosystem II; ABC, ATP-binding cassette; EPR, electron paramagnetic resonance; FZ, ferrozine; PDB, Protein Data Bank; contig, group of overlapping clones; sf, super-folder; TAT, twin-arginine translocase; TES, [tris(hydroxymethyl)methyl]-2-aminoethanesulfonic acid; OLE, overlap extension.

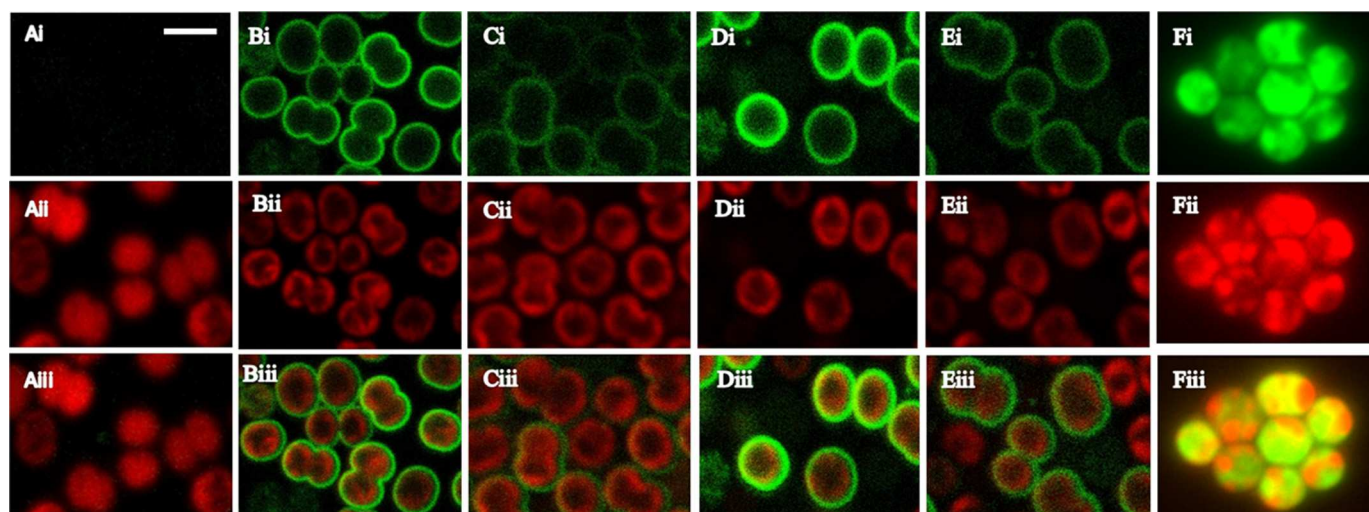


Figure 2. Localization of signal sequence-GFP constructs in *Synechocystis*. Using confocal microscopy the WT (A) was compared with strains expressing GFP fused to the signal sequences of the *E. coli* control TorA (B), *Synechocystis* FutA1 (C), *Synechocystis* FutA2 (D), and *Trichodesmium* Tery_3377 (E); the GFP control, *i.e.* without signal sequence, is shown in F. Imaging was performed under identical settings with excitation at 488 nm and is shown as GFP emission at 510–530 nm (panels *i*) and as autofluorescence (represented by phycocyanin) at 600–700 nm (panels *ii*); the merged images are shown in panels *iii*. Periplasmic localization of GFP is indicated by green fluorescent halos around the periphery of the cells in all strains (B–E) but not in WT (A) or the GFP control (F), with the latter showing cytosolic expression in absence of a signal peptide. The scale bar represents 1.5 μm .

therefore not possible. In addition, like the *Synechocystis futA1* and *futA2* genes, the Tery_3377 gene is located at an independent locus to genes encoding putative Fut ABC-transporter permease (FutB/Tery_3223) and ATPase subunits (FutC/Tery_3222), making functional inference from genomic context impossible.

Phylogenetic analysis was carried out to investigate grouping of Tery_3377 with IdiA/FutA homologs (Fig. 1). A multiple sequence alignment was constructed from Tery_3377, FutA1, and FutA2, along with homologs from range of cyanobacterial species, and this was used to generate a maximum likelihood phylogenetic tree. The *Synechocystis* FutA1 and FutA2 proteins are separated into distinct branches within the tree (branch support 0.97, approximate likelihood ratio test). Tery_3377 appears to be more closely related to the intracellular FutA1 protein than to FutA2. To confirm placement of the Tery_3377 protein within the phylogeny, we searched for homologs in other publicly available *Trichodesmium* genomes/metagenomes. No Tery_3377 homolog could be detected in the draft genome of *Trichodesmium theibautii* H94 (Bioproject PRJNA278659); however, this genome is known to be incomplete (28). A homolog was found in a metagenomic dataset from the Bermuda Atlantic Time Series (Bioproject PRJNA336846). This protein (encoded between nucleotides 342 and 1392 on contig 00877) clustered with Tery_3377 (Fig. 1).

The Tery_3377 signal peptide targets GFP to the periplasm

To investigate the cellular localization of Tery_3377, a synthetic gene encoding the predicted signal peptide (amino acids 1–31) and the first four residues of the mature protein (amino acids 32–35) fused to super-folder (sf)GFP was expressed in *Synechocystis* under the control of the *psbAII* promoter (Table S1 and Fig. S1). For comparison, the predicted *Synechocystis* FutA1 and FutA2 signal peptides were also fused to sfGFP and expressed from the *psbAII* promoter. The *Escherichia coli* TMAO reductase (TorA) signal peptide that has previously

been shown to transport GFP/yellow fluorescent protein into the periplasm of *Synechocystis* was used as a positive control, and sfGFP alone, *i.e.* without signal sequence, acted as a marker of cytoplasmic expression (29, 30).

The strains were visualized by confocal microscopy. Excitation of WT cells at 488 nm does not result in fluorescence emission in the GFP channel at 510–530 nm, but prominent autofluorescence from thylakoid membrane-localized photosynthetic pigments was observed when emission was monitored at 600–700 nm (Fig. 2A), as expected. Fusion of sfGFP to the TorA (Fig. 2B) or FutA2 (Fig. 2D) signal peptide results in bright fluorescent halos that surround the autofluorescence signal in merged images, indicating translocation of GFP across the cytoplasmic membrane to the periplasm. It is perhaps surprising that the FutA1 signal peptide also appears to localize some GFP to the periplasm or cytoplasmic membranes, albeit to a lesser extent than with the TorA or FutA2 fusions (Fig. 2C). Previous studies have suggested that FutA1 is mainly associated with thylakoid membranes, although it has been detected in the plasma membrane (26).

Fusion of the Tery_3377 signal peptide to GFP results in distinct halos (Fig. 2E), although this is not as clear as for the TorA and FutA2 signal peptides (Fig. 2, B and D) and also showed similarity to the FutA1 fusion (Fig. 2C). We changed the twin arginine residues in the Tery_3377 signal peptide to lysines, which prevented export of GFP and showed that the WT Tery_3377 signal peptide is recognized and exported by the twin-arginine translocase (TAT) system (Fig. S2). Immunoblots with an anti-GFP antibody identified a protein ~3 kDa larger than sfGFP in the stain with the mutated signal peptide, consistent with the presence of the uncleaved signal peptide (Fig. S3A). In the strain producing just sfGFP without a signal peptide, clear fluorescence signal mapping to the cytoplasm was observed (Fig. 2F), as expected and as reported previously for yellow fluorescent protein (30).

Structure and function of *Trichodesmium Tery_3377*

These results indicate that the *Tery_3377* signal peptide can translocate GFP to the periplasm using the TAT system. Both of the native *Synechocystis* FutA signal peptides also result in some degree of cytoplasmic membrane or periplasmic localization of GFP. Based on previous work FutA1 is considered to be predominantly intracellular; hence this result is unexpected. It is likely that the mature protein sequences also play a role in cellular localization, but attempts to investigate this in strains in which GFP was fused to the full proteins rather than just the signal peptides were unsuccessful because the strains were either genetically unstable or GFP was cleaved from the protein (data not shown).

Tery_3377 is involved in Fe^{3+} transport across the cell membrane

The signal peptide fusions indicated that *Tery_3377* is at least partly localized in the periplasm, presumably functioning as the periplasmic binding protein component of a ferric uptake ABC transporter. To gain further insight into the functional role of *Tery_3377*, the gene was codon-optimized for expression in *Synechocystis* and integrated at the *psbAII* locus in $\Delta futA1$ and $\Delta futA2$ *Synechocystis* mutants. Production of *Tery_3377* was confirmed by immunoblotting with the anti-IdiA antibody (raised against *Synechococcus elongatus* PCC 6302 IdiA) but was not detected using an antibody against *Synechocystis* FutA2 (Fig. 3B).

The high affinity iron ligand ferrozine (FZ) scavenges Fe^{2+} and cannot penetrate the cell membrane and thus is hypothesized to cause an iron-stress phenotype through reduction of ferrous iron uptake through the FeoAB system (31–33). This effect would be expected to be more severe in strains in which ferric iron uptake is also reduced, such as the $\Delta futA2$ strain. Experiments were performed in biological triplicate, and differences between FZ-treated and nontreated cells for each strain were determined for growth and photosynthetic efficiency (Fig. 3). A reduction in photosynthetic efficiency (F_v/F_m) is expected under iron stress because of the essential role of iron in the photosynthetic electron transport chain (4, 5).

In the presence of FZ, growth rates were significantly reduced by 13% in the WT ($P < 0.01$) and 15% in the $\Delta futA1$ strain ($P < 0.05$; Fig. 3A), whereas the $\Delta futA2$ mutant lacking the Fe^{3+} transporter showed the greatest response, as expected (32% reduction, $P < 0.01$). The reduction in growth rate by FZ in both mutants was not as apparent when *Tery_3377* was introduced to complement the knockout strains $\Delta futA1$ and $\Delta futA2$, suggesting that *Tery_3377* enables the cells to acquire ferric iron when ferrous iron is bound by FZ. Growth in presence of FZ also caused a reduction in photosynthetic efficiency (F_v/F_m) that was largest for $\Delta futA2$ (34%). The negative effect on the $\Delta futA2$ phenotype was again alleviated in the *tery_3377* complementation strain (Fig. 3B). In contrast, the reduction in photosynthetic efficiency in the $\Delta futA1$ knockout is less severe than WT.

Tery_3377 binds ferric (Fe^{3+}) iron

Recombinant *Tery_3377* with a C-terminal His tag was overproduced in *E. coli* and purified to investigate its affinity and binding of iron species. After incubation with ammonium

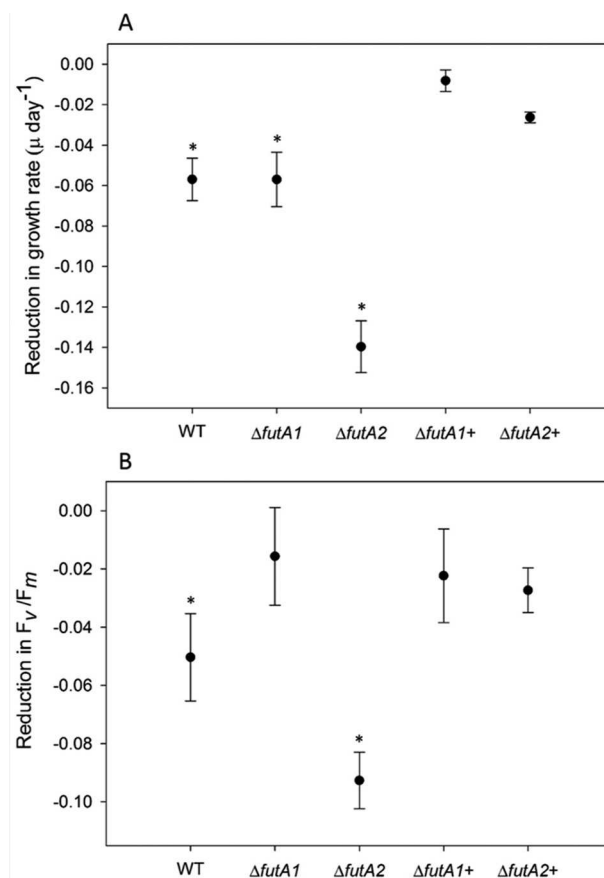


Figure 3. Reduction in growth and photosynthetic efficiency of strains grown in the presence of ferrozine. A and B, the decrease in growth rates measured as μ (day^{-1}) (A) and photosynthetic efficiency measured as F_v/F_m (B) during exponential growth of *Synechocystis* in YBG11 medium when grown with and without the Fe^{2+} -binding ligand FZ. The data are presented for WT, $\Delta futA1$, and $\Delta futA2$ mutants and the same strains expressing the *Trichodesmium tery_3377* gene ($\Delta futA1+$ and $\Delta futA2+$). Error bars show the standard deviation from the mean of three biological replicates. Statistical significance (*) was assessed using the Student's *t* test ($P < 0.05$).

$Fe(II)$ sulfate under aerobic conditions, the *Tery_3377*–iron complex was isolated by size-exclusion chromatography to remove unbound iron. The purified protein–iron complex was analyzed by EPR spectroscopy to determine the oxidation state of the bound iron ligand. EPR spectra revealed an oxidized Fe^{3+} state present in the *Tery_3377* sample (Fig. 4). In addition to weaker signals between 800 and 1400 Gauss, a sharp and intense signal at ~ 1500 Gauss (equal to a *g* value of 4.3) was clearly observed. This *g* value (4.3) is indicative of a high-spin Fe^{3+} ion bound to *Tery_3377*. The typical fingerprint weaker signals are related to higher order spin transitions of this ferric iron.

Crystal structures of *Tery_3377* reveal pentacoordination of Fe^{3+}

To study Fe^{3+} binding by *Tery_3377*, the structure of the iron-bound protein was determined using X-ray crystallography (Table 1). The overall fold of *Tery_3377* assumes a classic small molecule ABC transporter substrate-binding domain fold, with two domains hinged over a substrate-binding cleft. The hinge region is formed by two short β -strands and connects the protein domains via a double cross-over between the

N (residues 34–133 and 266–349) and C termini (134–265). This type of structure places Tery_3377 among class IV iron-binding proteins (in keeping with Ref. 27) and allows for structural classification within cluster D of the substrate-binding domains (35, 36).

Iron substrate-binding domains of different classes differ in iron ligand coordination, determined by conserved interacting

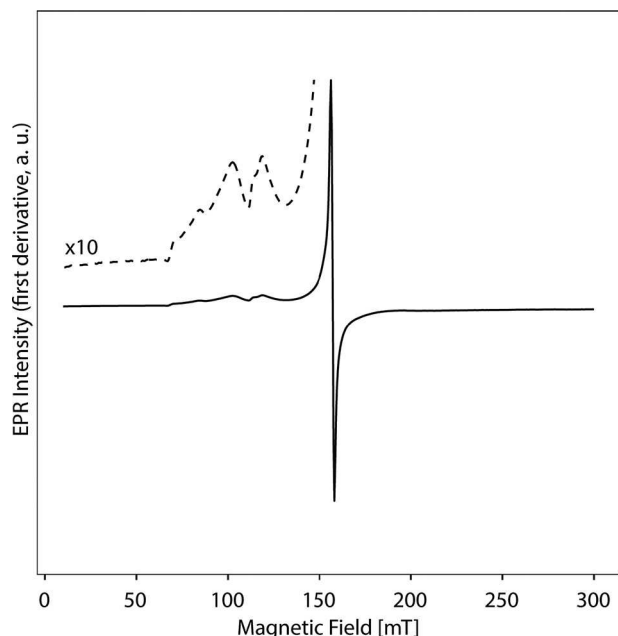


Figure 4. EPR spectrum of reconstituted Tery_3377 probing the iron center. Recombinant purified Tery_3377 from *T. erythraeum* ISM101 produced in *E. coli* was incubated with ammonium Fe(II) sulfate under aerobic conditions; the complex was repurified by size-exclusion chromatography to remove unbound iron. The EPR spectrum was collected from a sample with 0.55 mM protein concentration.

Table 1
Crystallographic analysis: data collection and refinement statistics

The values in parentheses refer to the highest resolution shell.

	Tery_3377-Ala	Tery_3377-Water	Tery_3377-Cit
PDB accession code	6G7N	6G7P	6G7Q
Data collection			
Space group	P2 ₁	P2 ₁	P2 ₁
Cell dimensions			
<i>a</i> , <i>b</i> , <i>c</i> (Å)	56.2, 83.2, 65.2	56.0, 82.9, 64.9	56.3, 102.0, 57.7
α , β , γ (°)	90, 95.20, 90	90, 95.20, 90	90, 112.85, 90
Resolution (Å)	29.26–1.1 (1.130–1.1)	29.11–1.5 (1.540–1.5)	28.64–1.2 (1.230–1.2)
<i>R</i> _{merge} (%)	0.04759 (0.3528)	0.04115 (0.2744)	0.07207 (0.8711)
<i>I</i> / σ (<i>I</i>)	11.83 (3.00)	16.22 (4.13)	11.63 (1.55)
<i>CC</i> _{1/2}	0.998 (0.765)	0.999 (0.917)	0.999 (0.679)
Completeness (%)	99.42 (99.56)	95.48 (94.11)	98.30 (99.17)
Redundancy	3.2 (3.0)	3.5 (3.6)	5.8 (5.6)
Refinement			
Resolution (Å)	29.26–1.1 (1.129–1.1)	29.11–1.5 (1.539–1.5)	28.58–1.2 (1.231–1.2)
No. reflections	227,890 (16772)	85,685 (6274)	181,790 (13467)
<i>R</i> _{work} (%)	0.1337 (0.2358)	0.1476 (0.1790)	0.1355 (0.2630)
<i>R</i> _{free} (%)	0.1512 (0.2377)	0.1739 (0.2050)	0.1648 (0.2840)
Monomers/AU	2	2	2
No. of atoms	6236	5656	6198
Protein	5250	5106	5193
Ligand/ion	24	11	49
Water	962	539	956
<i>B</i> -factors	16.42	18.12	17.88
Protein	15.24	17.90	16.46
Ligand/ion	27.24	34.35	26.75
Water	29.35	24.75	31.17
R.m.s. deviations			
Bond length (Å)	0.012	0.018	0.019
Bond angle (°)	1.57	1.89	2.01

amino-acid side chains of the substrate-binding domain, often involving tyrosine residues. In Tery_3377 three tyrosine residues, Tyr-144, Tyr-200, and Tyr-201, from the C-terminal domain contribute to iron binding. In the structure of Tery_3377-Ala (PDB entry 6G7N), determined at 1.1 Å resolution, a buffer molecule from the crystallization mixture occupies two coordination sites, giving rise to a pentacoordinated iron assigned as Fe³⁺ (Fig. 5A). The geometry observed is trigonal bipyramidal, with the buffer molecule alanine carboxyl group, Tyr-174 and Tyr-231, forming the trigonal plane with angles of 108°, 108°, and 144°. Tyr-230 and the amino group from the buffer alanine coordinate the axial iron positions.

Amino acid additives in the crystallization buffers lead to the most ordered and best diffracting crystals. However, Tery_3377 crystallized under a variety of conditions, including ones that lacked amino acid additives. We determined the structure of the protein crystallized with a monosaccharide additive mixture and found it was devoid of an iron-coordinating ligand in the binding site, with the iron instead coordinated by ordered water molecules (Fig. 5B). Comparison of the Tery_3377-water structure (PDB entry 6G7P) to the Tery_3377-Ala complex shows that water molecules W1 and W2 take the positions of the alanine amino and carboxylate groups of the alanine ligand, respectively (Fig. 5). Interestingly, in this complex an additional water molecule ligand (W3) is inserted between the coordinating oxygen atoms of W2 and Tyr-231. Compared with Tery_3377-Ala, where the observed angle between Tyr-231–O and alanine-carboxyl oxygen was measured as 144°, this angle is split into two angles of roughly 73° measured between Tyr-231–O, the inserted water molecule W3, and W2. Like in Tery_3377-Ala, Tyr-230 and water W1 occupy the axial coordination sites in Tery_3377-water.

Structure and function of *Trichodesmium* Tery_3377

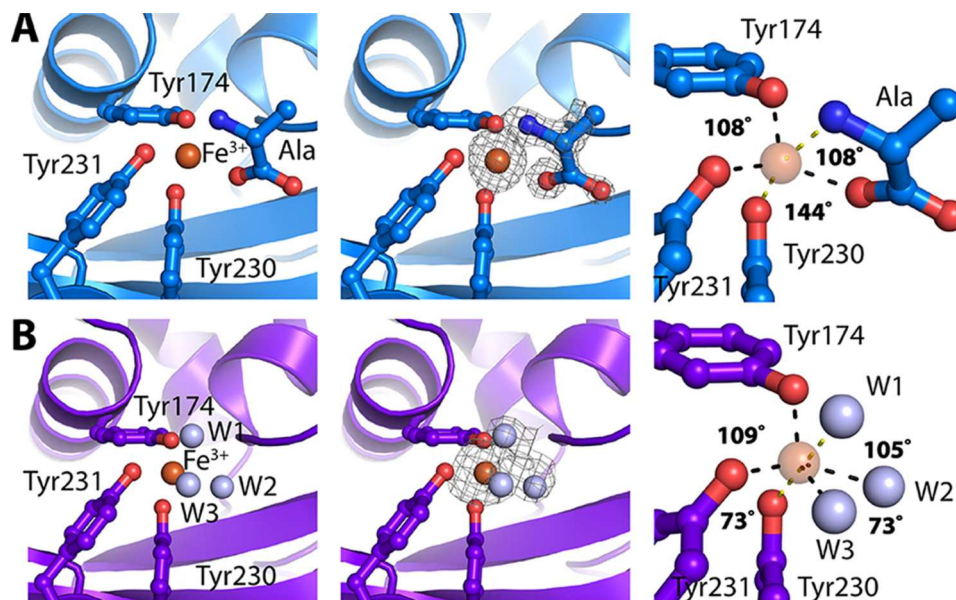


Figure 5. Structure analysis of Tery_3377. A, iron-binding site of Tery_3377-Ala with amino acid (Ala) ligand (left panel); the electron-density map shown (middle panel) is obtained after molecular replacement and subsequent refinement without ligands ($F_o - F_c$, contoured at 3σ); ligand coordination (right panel) shows iron in a trigonal bipyramidal geometry. Red, oxygen; blue, nitrogen; brown sphere, ferric ion; yellow dashes, H-bonds to axial coordination sites; gray dashes, H-bonds to equatorial coordination sites. B, iron-binding site of Tery_3377-water with water (W) ligands (left panel); the electron-density map shown (middle panel) is obtained after molecular replacement and subsequent refinement without ligands ($F_o - F_c$, contoured at 3σ); ligand coordination (right panel) shows iron in an octahedral geometry. Red, oxygen; brown sphere, ferric ion; gray sphere, water; yellow dashes, H-bonds to axial coordination sites; gray dashes, H-bonds to equatorial coordination sites.

To try and crystalline ligand-free Tery_3377 to examine structural changes upon iron binding, we citrate-treated Tery_3377 protein preparations prior to crystallization; citrate is known to chelate iron and was added to remove all iron from the protein preparation. The crystal structure (Tery_3377-Cit; PDB entry 6G7Q) traps the citrate molecule with bound iron in the substrate-binding cleft, where the iron is removed ~ 7 Å from the binding site (Fig. 6). The iron-binding site (pink sphere in Fig. 6) was free of metal, and the significance of this finding in the context of possible siderophore acquisition is discussed below.

Discussion

We have investigated the function and structure of *Trichodesmium* Tery_3377, an iron stress-induced protein (iron deficiency-induced A, IdiA) commonly used as an *in situ* marker of iron stress (15–17). Phylogenetic analysis (Fig. 1) groups Tery_3377 with the *Synechocystis* FutA1 protein, which has a suggested intracellular PSII protective function, rather than the FutA2 protein, a periplasmic protein with a role in iron transport. However, because of the high level of sequence identity of Tery_3377 to both FutA1 and FutA2 proteins and FutA1/2 proteins to one another, the function of these similar iron-binding proteins may be determined by their cellular localization. By fusion to sfGFP, Tery_3377 is shown to have a functional signal sequence for transport to the periplasm (Fig. 2) by the TAT system (Figs. S1 and S2). Consistent with this, Tery_3377 complements, the FZ induced the iron stress phenotype of the *Synechocystis* $\Delta futA2$ deletion strain (Fig. 3). These data support functional assignment of Tery_3377 as a subunit of an iron-uptake ABC transporter.

Expression of Tery_3377 also complements the more subtle phenotype of the $\Delta futA1$ *Synechocystis* mutant in the presence

of FZ. This may indicate the possibility of an additional intracellular function in PSII protection or alternatively result from increased ferric iron uptake by Tery_3377. Because localization data using FutA1 signal peptide GFP fusions resulted in some periplasmic localization (Fig. 2), FutA1 may have a role in iron uptake in addition to its reported intracellular function. Indeed, despite their apparently distinct cellular locations and functions, a *futA1/futA2* double mutant in *Synechocystis* has more severe iron-deficient growth and ferric iron uptake phenotypes than either single mutant, suggesting some degree of redundancy (20). In agreement with this, the phenotype of the double mutant is similar to that of mutants of the single copy Fut ABC-transporter permease (*futB*) and ATPase subunit (*futC*) genes (20). Hence, the IdiA/FutA family of proteins may commonly display a dual function that requires a broader reassessment across cyanobacteria.

EPR spectroscopy and structural analysis confirms that Tery_3377 binds iron in the ferric oxidation state, Fe³⁺ (Fig. 4). Tery_3377 crystallizes under various conditions, often requiring small-molecule additives. The best diffracting crystals were obtained with an additive mixture of amino acids (Fig. 5A). An amino acid ligand, alanine, is identified in the iron-binding cleft; the amino acid is ordered and coordinates the iron substrate. In contrast, other crystallization conditions, which did not show ligand coordination by organic molecules, gave less well-ordered crystals that diffracted to lower resolution and generally refined to higher *R* values, indicating a lower quality of the resulting models (Table 1). We also determined the structure where organic ligands are absent from the iron-binding site, with three water molecules coordinating the iron, in place of the two coordinating atoms seen with the alanine ligand structure (Fig. 5B).

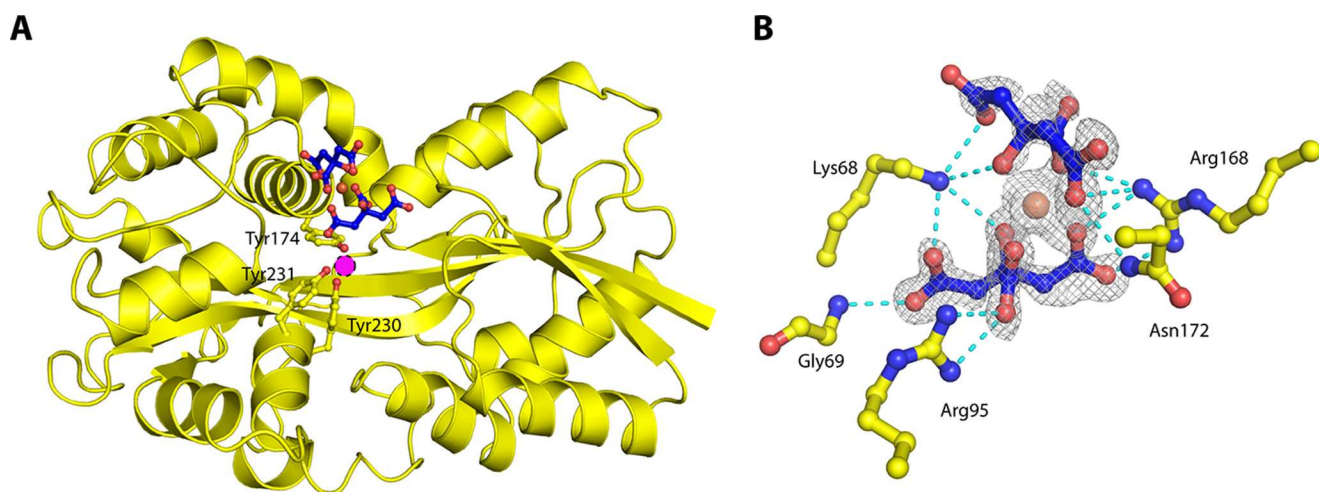


Figure 6. Iron-binding site and coordination of citrate molecules. *A*, the structure of Tery_3377-Cit. The fold is illustrated by the *yellow ribbon*, and the iron-binding site is shown by *sticks* representing the tyrosines shown in Fig. 5 (*yellow*) and two citrate molecules (*blue*). The iron coordinated by the two citrate molecules is shown as a *brown sphere*. The *magenta circle* indicates the position an iron ligand would occupy in iron-loaded Tery_3377. *B*, several protein amino acids, shown as *yellow sticks*, coordinate the citrate residues, shown in *blue*. The electron-density map is obtained after molecular replacement and subsequent refinement without ligands ($F_o - F_c$, contoured at 2σ). *Red*, oxygen; *brown*, ferric ion; *gray mesh*, electron density; *blue dashes*, coordinating interactions.

To determine the most likely coordination state of iron in Tery_3377, we superposed the Tery_3377-Ala structure with a classic closed conformation FutA2 structure (*Synechocystis* PCC6803 FutA2, PDB entry 2VP1) (Fig. 7A). The coordinating oxygen of the carboxylic acid moiety of the alanine ligand ideally superposes with a tyrosine side chain oxygen, whereas the amino nitrogen of the alanine ligand superimposes with a nitrogen from an interacting histidine ligand (Fig. 7, B and C). The two coordinating amino-acids in FutA2 are contributed by a loop that is brought into the vicinity of the iron-binding site by domain closure around the hinge that brings the two lobes of the substrate-binding domain closer together (37, 38) (Fig. 7A). Interestingly, this motif is conserved in Tery_3377, and such a domain closure, although not observed under any of our crystallization conditions, can be proposed. We conclude that the alanine ligand mimics this iron-binding mode, leading to a pentacoordinated state. This coordination state is corroborated by the low-temperature solution EPR spectroscopy, which revealed a strong signal at $g = 4.3$ and less intense higher-order transitions at higher g values, supporting generic class IV iron coordination by Tery_3377 in solution.

The observed binding of organic ligands together with iron may just be a fortuitous observation, but it might also have biological significance. It could be argued that the high concentrations of alanine present in crystallization mixtures out-competes interactions with the N-terminal iron-coordination residues His-43 and Tyr-44, thus leading to preferred crystallization of an open conformation. However, specific buffer molecules such as carbonate have previously been shown to coordinate iron in substrate-binding domains (39). Indeed, the binding site is large enough to fit a variety of amino acids in similar fashion to the shown alanine in Tery_3377-Ala. Hence, iron binding might concur with binding of different, larger molecules in the binding site. Nitrogen-containing molecules might enrich in the periplasm, creating a concentration gradient over the outer membrane. Additional support for the plasticity in the binding of Tery_3377 comes from the observation

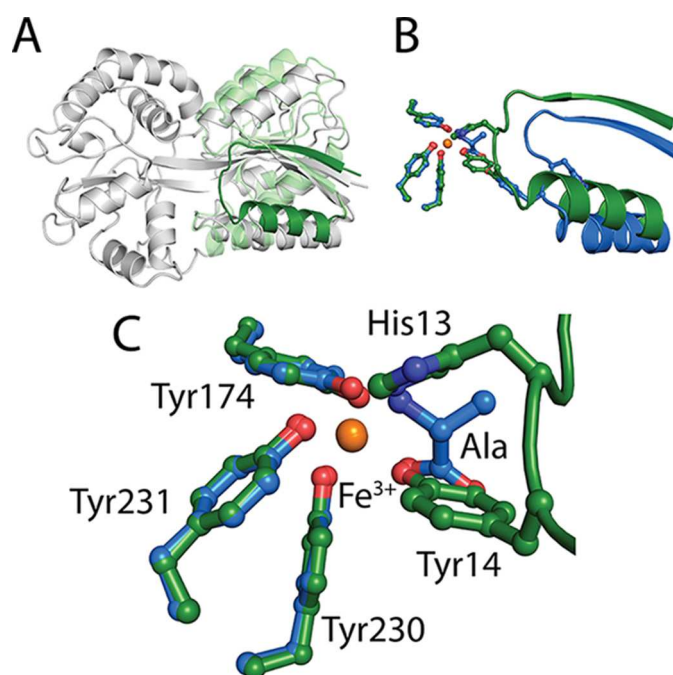


Figure 7. Analysis of iron coordination in Tery_3377. *A*, the open state of FutA2 from *Synechocystis* sp. PCC6803 is iron-free (*gray*). When superposed with the closed iron-bound form of FutA2 from *Synechocystis* sp. PCC6803 (Fe-FutA2), the C-terminal domains can be brought into perfect overlap, whereas the N-terminal domains reveal structural changes (*green* and *light green*) indicative of a closing of the substrate-binding cleft. Notably, a loop region contributing binding residues to the iron-binding sites is observed in a different position (*green*) to the open state. *B*, superposition of Tery_3377-Ala (*blue*) with Fe-FutA2 (*green*). The loop from the N-terminal domain brings iron coordinating tyrosine and histidine side chains into contact distance, allowing iron coordination. *C*, coordination site of superposed Tery_3377-Ala (*blue*) with iron-FutA2 (*green*). The equivalent amino acid residues to His-13 and Tyr-14, His-43, and Tyr-44 in Tery_3377 are not seen in contact with iron in either Tery_3377-Ala nor Tery_3377-water. However, the polar atoms from the alanine ligand in Tery_3377-Ala superpose well with the coordinating atoms of His-13 and Tyr-14. The three coordinating tyrosine residues originating from the C-terminal domains occupy the same position in Tery_3377-Ala and Fe-FutA2. Coordinating residues (shown as *sticks*) and ferric iron (*brown sphere*) are shown.

Structure and function of *Trichodesmium* Tery_3377

of bound citrate in the binding cleft, clearly indicating the potential for binding of organic compounds (Fig. 6). It is interesting to speculate that binding of organic ligands together with iron may represent a mechanism of siderophore recognition.

Summary

This study provides structural and mechanistic insight into a key protein important in iron acquisition and the iron stress response in the globally significant marine diazotroph *Trichodesmium*. These organisms are central to N_2 fixation, a highly significant process in the biogeochemical cycle, whose biogeography is determined by the availability of iron. Using heterologous expression in the model cyanobacteria *Synechocystis* PCC6803, we provide evidence that Tery_3377, a commonly used iron-limitation biomarker, is localized to the periplasm with a suggested FutA2 function as an iron-binding protein of an ABC transporter. However, Tery_3377 also complements deletion of FutA1, which could indicate that it also functions in protection of PSII, suggesting a potential dual function of Tery_3377 and more generally the IdlA/Fut family of proteins in cyanobacteria. Structural and spectroscopic characterization of recombinantly produced Tery_3377 confirms ferric iron binding under aerobic conditions. The structural data further show a remarkable plasticity of the substrate-binding cleft, allowing organic molecules and potentially siderophores to bind in addition to Fe^{3+} .

Experimental procedures

Protein phylogeny analysis

Maximum likelihood phylogenetic analysis of protein sequences of Tery_3377 homologs from *Synechocystis* and selected bacteria was performed to identify possible functional clusters. Homologs of the *Trichodesmium* Tery_3377 and two *Synechocystis* proteins FutA1 and FutA2 were identified by searching the NR protein database with BlastP (40). The top 10 closest hits were retained for each query sequence and clustered at 90% identity using CD-HIT (41) to reduce redundancy. For each cluster, one representative was retained for inclusion in the analysis. Homologs from *Prochlorococcus marinus* MIT 9301, *S. elongatus* PCC 6301 and PCC 7942, and *Anabaena* sp. PCC 7120 were also included in the analysis as representatives of important primary producers, and sequences from *Haemophilus influenzae* and *Neisseria meningitidis* were chosen to represent pathogens.

The online platform Phylogeny.fr (42, 43) was utilized in “a la carte” mode to create an analysis pipeline. Sequences were first aligned with T-coffee (v11.00.8cbe486, (44)), and the alignment was curated with G blocks (v0.91b) (45). Subsequently, a maximum likelihood phylogenetic tree was constructed using PhyML v3.1/3.0, (46), and an approximate likelihood ratio test was carried out to compute branch supports (approximate likelihood ratio test) (47). Finally, a graphical representation was produced with FigTree v1.4.3 (Institute of Evolutionary Biology, University of Edinburgh).

Growth conditions

Synechocystis strains (Table S2) were routinely grown in BG-11 medium (48) supplemented with 5 mM glucose and buff-

ered to pH 8.2 with 10 mM N-17 TES-KOH. Cultures were maintained at 30 °C with shaking at 150 rpm under constant illumination of $\sim 50 \mu\text{M}$ photons $\text{m}^{-2} \text{s}^{-1}$. For growth on plates, 1.5% (w/v) agar and 0.3% (w/v) sodium thiosulphate were added. Antibiotics were included as appropriate (Table S2). FZ growth experiments were carried out in iron (0.6 mM FeCl_3) YBG-11 media (recipe described in Ref. 49) at a FZ final concentration of 200 μM (FZ+) or no added FZ (FZ-). Growth was assessed under photoautotrophic conditions (no glucose), in triplicate cultures illuminated by 30 μM photons $\text{m}^{-2} \text{s}^{-1}$ of red light to minimize abiotic photoreduction of iron in the presence of FZ (50). *E. coli* (Table S2) was grown shaking (250 rpm) at 37 °C in LB (Luria-Bertani) broth with 100 $\mu\text{g ml}^{-1}$ ampicillin. The plates were set with 1.5% (w/v) agar.

Photosynthetic physiology

Photosynthetic efficiency of *Synechocystis* strains during FZ growth experiments was measured as F_v/F_m , an estimate of the apparent PSII photochemical quantum efficiency (51), using a FASTtrackTM MkII fast repetition rate fluorometer integrated with a FastActTM Laboratory system (Chelsea Technologies Group Ltd., Surrey, UK). The samples were dark adapted for 20 min prior to measurements. The presented results were calculated from the average of three technical replicates for each of three biological replicates.

Generation of *Synechocystis* strains

In this study, 1) pET21a was used for protein production in *E. coli*; 2) pACYC184 was used as a template to amplify the chloramphenicol resistance cassette; 3) pZEO was used as a template to amplify the zeocin resistance cassette; 4) pPD-FLAG was used as delivery vector for the introduction of genes into the *Synechocystis* genome in place of *psbAII*; and 5) pED151 was used for isolation of sfGFP.

For the generation of signal peptide fusions to sfGFP, DNA sequence corresponding to the predicted (in the case of *futA1*, *futA2*, Tery_3377) or known (*E. coli torA*) (52) signal sequence and the first 4 amino acid residues of the mature protein (as identified by SignalP v4.1/v3.0 sensitivity and TatP v1.0 servers (53, 54) (Table S1 and Fig. S1) was amplified from the respective organisms genomic DNA (for details of all primers used in this study see Table S3). Approximately 400 bp immediately preceding the *psbAII* gene was joined to each signal sequence by overlap extension (OLE)-PCR such that the ATG start codon of the signal sequence replaced the ATG start codon of *psbAII*. Using the same technique the chloramphenicol acetyl transferase (*cat*) gene from pACYC184 (New England Biolabs) was inserted between the coding sequence for sfGFP (55) and ~ 400 bp of sequence immediately downstream of *psbAII*. Finally, each *psbAII* upstream-signal sequence fragment was joined to the sfGFP-*cat-psbAII* downstream fragment, again using OLE-PCR. The *psbAII* locus is extensively utilized as a “neutral site” that will not result in polar effects following gene insertion and is commonly used for expression of recombinant genes (56).

To generate a variant of the Tery_3377 signal peptide in which the twin arginine residues were replaced by lysines (3377ss-KK-GFP), alternative primers were designed to anneal during OLE-PCR, and both contained the first 18 bp of the

Tery_3377 signal sequence with changed nucleotide sequence between positions 13 and 18 (AAA AAA in the place of AGA CGA), such that the translated sequence codes for two lysine residues in the place of the two arginine residues of the TAT system.

Synechocystis was transformed as described in Ref. 57 with selection on chloramphenicol ($8.5 \mu\text{g ml}^{-1}$). Genome copies were segregated by repeated streaking on BG11 plates with increasing antibiotic concentration up to $34 \mu\text{g ml}^{-1}$, and homozygous transformants were verified by PCR and sequencing (Eurofins MWG Operon, Ebersberg, Germany).

For the generation of slr1295 (ΔfutA1) and slr0513 (ΔfutA2) *Synechocystis* deletion mutants, the antibiotic resistance cassette for zeocin (ZeoR) from pZEO (58) or the *cat* gene were used. PCR products consisting of the sequence upstream of the *futA1/futA2* genes and the beginning of the ORF or the end of the ORF and downstream flanking DNA were amplified from *Synechocystis* genomic DNA. Using OLE-PCR, ZeoR or *cat* was inserted between the upstream and downstream PCR products to create a linear mutagenesis fragment. For *slr1295 (futA1)* the entire gene apart from the first 22 bp was replaced with the zeo cassette. For *slr0513 (futA2)* all but the first 66 bp and last 41 bp of the gene were replaced by the *cat* cassette. The deletion constructs were introduced into WT *Synechocystis* as described above, with selection and segregation on zeocin ($2.5\text{--}20 \mu\text{g ml}^{-1}$) or chloramphenicol ($8.5\text{--}34 \mu\text{g ml}^{-1}$). Full segregation of mutant strains was confirmed by PCR.

For expression of *tery_3377* in *Synechocystis*, the gene was codon-optimized (Integrated DNA Technologies Inc., Leuven, Belgium) and cloned into the NdeI/BglII sites of pPD-FLAG (56). Transformation of *Synechocystis* with the constructed plasmid integrates *tery_3377* into the *Synechocystis* genome such that expression is driven from the *psbAII* promoter and confers kanamycin resistance allowing selection of transformed cells using increasing concentrations of kanamycin ($10\text{--}40 \mu\text{g ml}^{-1}$). Segregation of transformants at the *psbAII* locus was confirmed by PCR, and the sequence of the gene was verified by sequencing, as above.

Fluorescence microscopy

Synechocystis cells producing sfGFP fusion proteins were visualized using a Leica SP5 LSCM confocal microscope (Leica Microsystems, Wetzlar, Germany) or a axioscope Z plus epifluorescence microscope (Zeiss, Oberkochen, Germany). For confocal microscopy, samples were excited at 488 nm, and emission was measured at 510–530 nm for sfGFP fluorescence or 600–700 nm for autofluorescence, as described in Ref. 59. For visualization of sfGFP by epifluorescence microscopy, excitation was set at 400–490 nm (max 441 nm), and emission was measured at 460–570 nm (max 485 nm).

EPR

Oxidized Tery_3377 ($550 \mu\text{M}$) was placed in EPR quartz tubes (Wilmad) and shock-frozen in liquid nitrogen. X-band continuous wave EPR spectra were recorded on a Bruker eleXsys E500 spectrometer using a standard rectangular Bruker EPR cavity (ER4102T) equipped with an Oxford helium flow cryostat (ESR900). The spectrometer operates at X-band (~ 9.4

GHz) frequency and uses a 1-mT modulation amplitude (peak to peak) and 2-milliwatt microwave power. The spectra were recorded at cryogenic temperatures (5–6 K). A typical spectrum was recorded in $\sim 15\text{--}30$ min.

Protein production, crystallization, and structure determination

To produce C-terminally His₆-tagged Tery_3377 in *E. coli*, the ORF (minus the putative sequence encoding the N-terminal signal peptide and stop codon) was amplified from the *Trichodesmium* genome. The resulting PCR product was digested and cloned into the NdeI/XhoI sites of pET21a(+) (Novagen). The sequence verified plasmid was introduced into *E. coli* BL21(DE3), and production of the recombinant protein was induced in cells grown to an A_{600} of 0.6 by addition of 0.4 mM isopropyl- β -D-thiogalactopyranoside, followed by growth for a further 4 h. The cells were harvested by centrifugation ($6000 \times g$, 20 min, 4 °C), resuspended in binding buffer (50 mM Tris, 200 mM NaCl, 5% glycerol, 20 mM imidazole), and broken (sonication for 10 s on, 30 s off; 2 min process time), and the cell-free extract was isolated as the supernatant following centrifugation ($200,000 \times g$, 45 min, 4 °C). His-tagged Tery_3377 was purified by affinity chromatography (1-ml HisTrap HP columns; GE Healthcare) and size-exclusion chromatography (HiLoad 16/60 Superdex 200; GE Healthcare).

Tery_3377 crystals were obtained in space group P2₁ with two molecules in the asymmetric unit with slightly different packing between iron-bound and iron-free forms of Tery_3377. Hanging-drop vapor diffusion used conditions based on or optimized from the Morpheus screen (Molecular Dimensions). The reservoir composition leading to Tery_3377-Ala crystals was 0.1 M amino acids mix, 0.1 M buffer system 2, pH 7.5, 50% precipitant mix 1. Tery_3377-Ala data were collected at the Diamond Light Source Beamline I02 to a resolution of 1.1 Å. Tery_3377-water crystals were obtained with a reservoir composition of 0.12 M monosaccharides mix, 0.1 M buffer system 2, pH 7.5, 50% precipitant mix 1. Tery_3377-water data were collected at the Diamond Light Source Beamline I02 to a resolution of 1.5 Å. Tery_3377-Cit crystals were obtained with a reservoir composition of 0.1 M carboxylic acids mix, 0.1 M buffer system 2, pH 7.5, 50% precipitant mix 1. Tery_3377-Cit data were collected at European Synchrotron Radiation Facility Beamline ID30B to resolution of 1.2 Å.

The XDS package (60) was used to index, integrate, and scale diffraction data. The structures have been determined by molecular replacement with Phaser (61) using coordinates of apo-FutA2 from *Synechocystis* (PDB entry 2VOZ) (21) and were further refined with REFMAC5 (62). During refinement, hydrogens were added in their riding positions, and refinement was iterated with water building and model correction in Coot (63).

Immunoblotting

Synechocystis cells were resuspended in 100 μl of 10 mM Tris-HCl, pH 7.3, and heated for 5 min at 100 °C followed by centrifugation at 10,000 rpm for 5 min at 4 °C. The samples were analyzed by SDS-PAGE on 4–12% NuPAGE acrylamide gradient gels (Life Technologies). Protein was blotted onto nitrocel-

lulose membrane, which was blocked for 1 h in Tris-buffered saline with Tween 20 (TSB-T) and 2% ECL Advance blocking reagent (GE Healthcare). Antibody incubations (1 h) and membrane washes were performed in TBS-T. Anti-IdiA and anti-Slr0513 (FutA2) antisera were a kind gift from E. Pistorius (24, 34) and were used at concentrations of 1:5000 and 1:10000 respectively. Following application of ECL Advance detection reagent (GE Healthcare), chemiluminescence was visualized using a VersaDoc™ CCD imager (Bio-Rad).

Author contributions—D. P., M. M. M., A. H., A. J. B., T. S. B., and I. T. formal analysis; D. P., M. M. M., A. H., T. S. B., and I. T. validation; D. P., M. M. M., A. H., A. J. B., and I. T. investigation; D. P. and M. M. M. visualization; D. P., M. M. M., A. H., T. S. B., and I. T. writing-original draft; A. H., F. M., and I. T. conceptualization; A. H., C.M.M., T. S. B., and I. T. supervision; A. J. B. and F. M. methodology; F. M. and I. T. data curation.

Acknowledgments—We thank Chris Holes of the macromolecular crystallization facility at the University of Southampton, staff at the Diamond Light Source, and the European Synchrotron Radiation Facility for access and excellent user support through proposals MX11945 and MX1848, respectively. We thank staff at the Biomedical Imaging Unit, Southampton General Hospital for assistance with confocal microscopy.

References

- Raven, J. A., Evans, M. C., and Korb, R. E. (1999) The role of trace metals in photosynthetic electron transport in o₂-evolving organisms. *Photosynth. Res.* **60**, 111–150 [CrossRef](#)
- Blaby-Haas, C. E., and Merchant, S. S. (2012) The ins and outs of algal metal transport. *Biochim. Biophys. Acta* **1823**, 1531–1552 [CrossRef](#) [Medline](#)
- Shi, T., Sun, Y., and Falkowski, P. G. (2007) Effects of iron limitation on the expression of metabolic genes in the marine cyanobacterium *Trichodesmium erythraeum* ims101. *Environ. Microbiol.* **9**, 2945–2956 [CrossRef](#) [Medline](#)
- Richier, S., Macey, A. I., Pratt, N. J., Honey, D. J., Moore, C. M., and Bibby, T. S. (2012) Abundances of iron-binding photosynthetic and nitrogen-fixing proteins of *Trichodesmium* both in culture and in situ from the North Atlantic. *PLoS One* **7**, e35571 [CrossRef](#) [Medline](#)
- Snow, J. T., Polyviou, D., Skipp, P., Christmas, N. A., Hitchcock, A., Geider, R., Moore, C. M., and Bibby, T. S. (2015) Quantifying integrated proteomic responses to iron stress in the globally important marine diazotroph *Trichodesmium*. *PLOS One* **10**, e0142626 [CrossRef](#) [Medline](#)
- Moore, J., and Braucher, O. (2007) Observations of dissolved iron concentrations in the world ocean: implications and constraints for ocean biogeochemical models. *Biogeosci. Discuss.* **4**, 1241–1277 [CrossRef](#)
- Rubin, M., Berman-Frank, I., and Shaked, Y. (2011) Dust- and mineral-iron utilization by the marine dinitrogen-fixing *Trichodesmium*. *Nat. Geosci.* **4**, 529–534 [CrossRef](#)
- Hansel, C. M., Buchwald, C., Ossolinski, J., Dyhrman, S., Van Mooy, B., Polyviou, D., et al. (2016) Dynamics of extracellular superoxide production by *Trichodesmium* colonies from the sargasso sea. *Limnol. Oceanogr.* **61**, 1188–1200 [CrossRef](#)
- Falkowski, P. G. (1997) Evolution of the nitrogen cycle and its influence on the biological sequestration of CO₂ in the ocean. *Nature* **387**, 272 [CrossRef](#)
- Capone, D. G., Zehr, J. P., Paerl, H. W., Bergman, B., and Carpenter, E. J. (1997) *Trichodesmium*, a globally significant marine cyanobacterium. *Science* **276**, 1221–1229 [CrossRef](#)
- Westberry, T. K., and Siegel, D. A. (2006) Spatial and temporal distribution of *Trichodesmium* blooms in the world's oceans. *Global Biogeochem. Cycles* **20**, [CrossRef](#)
- Achilles, K. M., Church, T. M., Wilhelm, S. W., Luther, G. W., and Hutchins, D. A. (2003) Bioavailability of iron to *Trichodesmium* colonies in the western subtropical Atlantic Ocean. *Limnol. Oceanogr.* **48**, 2250–2255 [CrossRef](#)
- Webb, E. A., Moffett, J. W., and Waterbury, J. B. (2001) Iron stress in open-ocean cyanobacteria (*Synechococcus*, *Trichodesmium*, and *Crocosphaera* spp.): identification of the idia protein. *Appl. Environ. Microbiol.* **67**, 5444–5452 [CrossRef](#) [Medline](#)
- Singh, A. K., McIntyre, L. M., and Sherman, L. A. (2003) Microarray analysis of the genome-wide response to iron deficiency and iron reconstitution in the cyanobacterium *Synechocystis* sp. PCC 6803. *Plant Physiol.* **132**, 1825–1839 [CrossRef](#) [Medline](#)
- Webb, E. A., Jakuba, R. W., Moffett, J. W., and Dyhrman, S. T. (2007) Molecular assessment of phosphorus and iron physiology in *Trichodesmium* populations from the western central and western South Atlantic. *Limnol. Oceanogr.* **52**, 2221–2232 [CrossRef](#)
- Rivers, A. R., Jakuba, R. W., and Webb, E. A. (2009) Iron stress genes in marine *Synechococcus* and the development of a flow cytometric iron stress assay. *Environ. Microbiol.* **11**, 382–396 [CrossRef](#) [Medline](#)
- Chappell, P. D., and Webb, E. A. (2010) A molecular assessment of the iron stress response in the two phylogenetic clades of *Trichodesmium*. *Environ. Microbiol.* **12**, 13–27 [CrossRef](#) [Medline](#)
- Michel, K.-P., and Pistorius, E. K. (2004) Adaptation of the photosynthetic electron transport chain in cyanobacteria to iron deficiency: the function of idia and isia. *Physiol. Plant.* **120**, 36–50 [CrossRef](#) [Medline](#)
- Exss-Sonne, P., Tölle, J., Bader, K. P., Pistorius, E. K., and Michel, K.-P. (2000) The idia protein of *Synechococcus* sp. PCC 7942 functions in protecting the acceptor side of photosystem II under oxidative stress. *Photosynth. Res.* **63**, 145–157 [CrossRef](#) [Medline](#)
- Katoh, H., Hagino, N., and Ogawa, T. (2001) Iron-binding activity of futA1 subunit of an abc-type iron transporter in the cyanobacterium *Synechocystis* sp. strain PCC 6803. *Plant Cell Physiol.* **42**, 823–827 [CrossRef](#) [Medline](#)
- Badarau, A., Firbank, S. J., Waldron, K. J., Yanagisawa, S., Robinson, N. J., Banfield, M. J., and Dennison, C. (2008) Futa2 is a ferric binding protein from *Synechocystis* PCC 6803. *J. Biol. Chem.* **283**, 12520–12527 [CrossRef](#) [Medline](#)
- Kranzler, C., Lis, H., Finkel, O. M., Schmetterer, G., Shaked, Y., and Keren, N. (2014) Coordinated transporter activity shapes high-affinity iron acquisition in cyanobacteria. *ISME J.* **8**, 409–417 [CrossRef](#) [Medline](#)
- Fulda, S., Huang, F., Nilsson, F., Hagemann, M., and Norling, B. (2000) Proteomics of *Synechocystis* sp. strain PCC 6803. *Eur. J. Biochem.* **267**, 5900–5907 [CrossRef](#) [Medline](#)
- Tölle, J., Michel, K.-P., Kruij, J., Kahmann, U., Preisfeld, A., and Pistorius, E. K. (2002) Localization and function of the idia homologue slr1295 in the cyanobacterium *Synechocystis* sp. strain PCC 6803. *Microbiology* **148**, 3293–3305 [CrossRef](#) [Medline](#)
- Waldron, K. J., Tottey, S., Yanagisawa, S., Dennison, C., and Robinson, N. J. (2007) A periplasmic iron-binding protein contributes toward inward copper supply. *J. Biol. Chem.* **282**, 3837–3846 [Medline](#)
- Huang, F., Parmryd, I., Nilsson, F., Persson, A. L., Pakrasi, H. B., Andersson, B., and Norling, B. (2002) Proteomics of *Synechocystis* sp. strain PCC 6803 identification of plasma membrane proteins. *Mol. Cell. Proteomics* **1**, 956–966 [CrossRef](#) [Medline](#)
- Wang, S., Ogata, M., Horita, S., Ohtsuka, J., Nagata, K., and Tanokura, M. (2014) A novel mode of ferric ion coordination by the periplasmic ferric ion-binding subunit fbpa of an abc-type iron transporter from thermophilus hb8. *Acta Crystallogr. D Biol. Crystallogr.* **70**, 196–202 [CrossRef](#) [Medline](#)
- Walworth, N., Pfreundt, U., Nelson, W. C., Mincer, T., Heidelberg, J. F., Fu, F., Waterbury, J. B., Glavina del Rio, T., Goodwin, L., Kyrpides, N. C., Land, M. L., Woyke, T., Hutchins, D. A., Hess, W. R., and Webb, E. A. (2015) *Trichodesmium* genome maintains abundant, widespread noncoding dna in situ, despite oligotrophic lifestyle. *Proc. Natl. Acad. Sci. U.S.A.* **112**, 4251–4256 [CrossRef](#) [Medline](#)
- Spence, E., Sarcina, M., Ray, N., Möller, S. G., Mullineaux, C. W., and Robinson, C. (2003) Membrane-specific targeting of green fluorescent

- protein by the tat pathway in the cyanobacterium *Synechocystis* PCC 6803. *Mol. Microbiol.* **48**, 1481–1489 [CrossRef Medline](#)
30. MacGregor-Chatwin, C., Sener, M., Barnett, S. F. H., Hitchcock, A., Barnhart-Dailey, M. C., Maghlaoui, K., Barber, J., Timlin, J. A., Schulten, K., and Hunter, C. N. (2017) Lateral segregation of photosystem I in cyanobacterial thylakoids. *Plant Cell* **29**, 1119–1136 [CrossRef Medline](#)
 31. Kustka, A. B., Shaked, Y., Milligan, A. J., King, D. W., and Morel, F. M. (2005) Extracellular production of superoxide by marine diatoms: contrasting effects on iron redox chemistry and bioavailability. *Limnol. Oceanogr.* **50**, 1172–1180 [CrossRef](#)
 32. Shaked, Y., Kustka, A. B., and Morel, F. M. (2005) A general kinetic model for iron acquisition by eukaryotic phytoplankton. *Limnol. Oceanogr.* **50**, 872–882 [CrossRef](#)
 33. Garg, S., Rose, A. L., Godrant, A., and Waite, T. D. (2007) Iron uptake by the ichthyotoxic *Chattonella marina* (Raphidophyceae): impact of superoxide generation. *J. Phycol.* **43**, 978–991 [CrossRef](#)
 34. Michel, K.-P., and Pistorius, E. K. (1992) Isolation of a photosystem II associated 36 kDa polypeptide and an iron-stress 34 kDa polypeptide from thylakoid membranes of the cyanobacterium *synechococcus* PCC 6301 grown under mild iron deficiency. *Z. Naturforsch. C* **47**, 867–874 [CrossRef](#)
 35. Berntsson, R. P., Smits, S. H., Schmitt, L., Slotboom, D.-J., and Poolman, B. (2010) A structural classification of substrate-binding proteins. *FEBS Lett.* **584**, 2606–2617 [CrossRef Medline](#)
 36. Scheepers, G. H., Lycklama, A., Nijeholt, J. A., and Poolman, B. (2016) An updated structural classification of substrate-binding proteins. *FEBS Lett.* **590**, 4393–4401 [CrossRef Medline](#)
 37. Tom-Yew, S. A., Cui, D. T., Bekker, E. G., and Murphy, M. E. (2005) Anion-independent iron coordination by the *Campylobacter jejuni* ferric binding protein. *J. Biol. Chem.* **280**, 9283–9290 [CrossRef Medline](#)
 38. Koropatkin, N., Randich, A. M., Bhattacharyya-Pakrasi, M., Pakrasi, H. B., and Smith, T. J. (2007) The structure of the iron-binding protein, futa1, from *Synechocystis* 6803. *J. Biol. Chem.* **282**, 27468–27477 [CrossRef Medline](#)
 39. Shouldice, S. R., Skene, R. J., Dougan, D. R., Snell, G., McRee, D. E., Schryvers, A. B., and Tari, L. W. (2004) Structural basis for iron binding and release by a novel class of periplasmic iron-binding proteins found in gram-negative pathogens. *J. Bacteriol.* **186**, 3903–3910 [CrossRef Medline](#)
 40. Altschul, S. F., Gish, W., Miller, W., Myers, E. W., and Lipman, D. J. (1990) Basic local alignment search tool. *J. Mol. Biol.* **215**, 403–410 [CrossRef Medline](#)
 41. Li, W., and Godzik, A. (2006) Cd-hit: a fast program for clustering and comparing large sets of protein or nucleotide sequences. *Bioinformatics* **22**, 1658–1659 [CrossRef Medline](#)
 42. Dereeper, A., Guignon, V., Blanc, G., Audic, S., Buffet, S., Chevenet, F., Dufayard, J.-F., Guindon, S., Lefort, V., Lescot, M., Claverie, J. M., and Gascuel, O. (2008) Phylogeny. fr: robust phylogenetic analysis for the non-specialist. *Nucleic Acids Res.* **36**, W465–W469 [CrossRef Medline](#)
 43. Dereeper, A., Audic, S., Claverie, J.-M., and Blanc, G. (2010) Blast-explorer helps you building datasets for phylogenetic analysis. *BMC Evol. Biol.* **10**, 8 [CrossRef Medline](#)
 44. Notredame, C., Higgins, D. G., and Heringa, J. (2000) T-coffee: A novel method for fast and accurate multiple sequence alignment. *J. Mol. Biol.* **302**, 205–217 [CrossRef Medline](#)
 45. Castresana, J. (2000) Selection of conserved blocks from multiple alignments for their use in phylogenetic analysis. *Mol. Biol. Evol.* **17**, 540–552 [CrossRef Medline](#)
 46. Guindon, S., and Gascuel, O. (2003) A simple, fast, and accurate algorithm to estimate large phylogenies by maximum likelihood. *Syst. Biol.* **52**, 696–704 [CrossRef Medline](#)
 47. Anisimova, M., and Gascuel, O. (2006) Approximate likelihood-ratio test for branches: a fast, accurate, and powerful alternative. *Syst. Biol.* **55**, 539–552 [CrossRef Medline](#)
 48. Rippka, R., Deruelles, J., Waterbury, J. B., Herdman, M., and Stanier, R. Y. (1979) Generic assignments, strain histories and properties of pure cultures of cyanobacteria. *Microbiology* **111**, 1–61 [CrossRef](#)
 49. Shcolnick, S., Shaked, Y., and Keren, N. (2007) A role for mrga, a dps family protein, in the internal transport of Fe in the cyanobacterium *Synechocystis* sp. PCC 6803. *Biochim. Biophys. Acta* **1767**, 814–819 [CrossRef Medline](#)
 50. Kranzler, C., Lis, H., Shaked, Y., and Keren, N. (2011) The role of reduction in iron uptake processes in a unicellular, planktonic cyanobacterium. *Environ. Microbiol.* **13**, 2990–2999 [CrossRef Medline](#)
 51. Kolber, Z. S., Prasil, O., and Falkowski, P. G. (1998) Measurements of variable chlorophyll fluorescence using fast repetition rate techniques: defining methodology and experimental protocols. *Biochim. Biophys. Acta* **1367**, 88–106 [CrossRef Medline](#)
 52. Thomas, J. D., Daniel, R. A., Errington, J., and Robinson, C. (2001) Export of active green fluorescent protein to the periplasm by the twin-arginine translocase (TAT) pathway in *Escherichia coli*. *Mol. Microbiol.* **39**, 47–53 [CrossRef Medline](#)
 53. Bendtsen, J. D., Nielsen, H., Widdick, D., Palmer, T., and Brunak, S. (2005) Prediction of twin-arginine signal peptides. *BMC Bioinformatics* **6**, 167 [CrossRef Medline](#)
 54. Petersen, T. N., Brunak, S., von Heijne, G., and Nielsen, H. (2011) Signalp 4.0: discriminating signal peptides from transmembrane regions. *Nat. Methods* **8**, 785–786 [CrossRef Medline](#)
 55. Pédelacq, J.-D., Cabantous, S., Tran, T., Terwilliger, T. C., and Waldo, G. S. (2006) Engineering and characterization of a superfolder green fluorescent protein. *Nat. Biotechnol.* **24**, 79–88 [CrossRef Medline](#)
 56. Hollingshead, S., Kopecná, J., Jackson, P. J., Canniffe, D. P., Davison, P. A., Dickman, M. J., Sobotka, R., and Hunter, C. N. (2012) Conserved chloroplast open-reading frame ycf54 is required for activity of the magnesium protoporphyrin monomethylester oxidative cyclase in *Synechocystis* PCC 6803. *J. Biol. Chem.* **287**, 27823–27833 [CrossRef Medline](#)
 57. Williams, J. G. (1988) [85] construction of specific mutations in photosystem II photosynthetic reaction center by genetic engineering methods in *Synechocystis* 6803. *Methods Enzymol.* **167**, 766–778 [CrossRef](#)
 58. Cereda, A., Hitchcock, A., Symes, M. D., Cronin, L., Bibby, T. S., and Jones, A. K. (2014) A bioelectrochemical approach to characterize extracellular electron transfer by *Synechocystis* sp. PCC 6803. *PLoS One* **9**, e91484 [CrossRef Medline](#)
 59. Aldridge, C., Spence, E., Kirkilionis, M. A., Frigerio, L., and Robinson, C. (2008) Tat-dependent targeting of rieske iron-sulphur proteins to both the plasma and thylakoid membranes in the cyanobacterium *Synechocystis* PCC 6803. *Mol. Microbiol.* **70**, 140–150 [CrossRef Medline](#)
 60. Kabsch, W. (2010) XDS. *Acta Crystallogr. D Biol. Crystallogr.* **66**, 125–132 [CrossRef Medline](#)
 61. McCoy, A. J., Grosse-Kunstleve, R. W., Adams, P. D., Winn, M. D., Storoni, L. C., and Read, R. J. (2007) Phaser crystallographic software. *J. Appl. Crystallogr.* **40**, 658–674 [CrossRef Medline](#)
 62. Murshudov, G. N., Vagin, A. A., and Dodson, E. J. (1997) Refinement of macromolecular structures by the maximum-likelihood method. *Acta Crystallogr. D Biol. Crystallogr.* **53**, 240–255 [CrossRef Medline](#)
 63. Emsley, P., and Cowtan, K. (2004) Coot: model-building tools for molecular graphics. *Acta Crystallogr. D Biol. Crystallogr.* **60**, 2126–2132 [CrossRef Medline](#)